Applied Thermal Engineering 153 (2019) 739–747

Contents lists available at ScienceDirect

Applied Thermal Engineering

journal homepage: www.elsevier.com/locate/apthermeng

Research Paper

Numerical study of flow boiling in an intermediate-scale vertical tube under low heat flux

Xuan Yin[a], Yongsheng Tian[b], Dan Zhou[c], Naihua Wang[a,*]

[a] Institute of Thermal Science & Engineering, Shandong University, Jinan 250061, China
[b] School of Thermal Engineering, Shandong Jianzhu University, Jinan 250101, China
[c] Wolfson School of Mechanical, Electrical and Manufacturing Engineering, Loughborough University, UK

HIGHLIGHTS

- A flow boiling model in an intermediate-scale vertical tube is constructed.
- The characteristics of the flow pattern rely on the height of the tube and low heat flux.
- The dynamic characteristics of flow boiling are analyzed.
- The heat transfer is enhanced with the increase in height.

ARTICLE INFO

Keywords:
Flow boiling
Intermediate-scale vertical tube
Numerical simulation
VOF

ABSTRACT

This article numerically investigates the flow boiling behavior in an intermediate-scale vertical tube for an evaporator of a separated type heat pipe. In this study, the volume of fluid (VOF) model and the vapor-liquid phase change model (according to a user defined function) are used to build a numerical model of a single vertical tube with a 50 mm inner diameter and 5000 mm length for simulating the flow regime. Different two-phase flow characteristics are present in the vertical tube working in low heat flux. We analyze the bubble movement and classify the two-phase flow regimes in an intermediate-scale vertical tube into four patterns: bubbly flow, cap flow, slug flow and churn flow. Furthermore, the local characteristic of boiling heat transfer along the tube and the effect of the bubble regimes on the heat transfer are studied. The results indicate that saturated nucleate boiling is the dominant boiling form under low heat flux.

1. Introduction

As a device with high heat transfer performance, the separated type heat pipe can transfer a large amount of heat through a small cross-sectional area for long-distance transmission without an external power supply. This type of heat pipe is widely used in the cooling of electronic devices [1], data center energy saving [2], and so on. Recently, passive cooling systems, such as passive containment cooling system (PCCS) [3,4] and passive cooling of spent fuel pool [5] have been applied to the third generation of nuclear power reactors to improve their safety and reliability. The containment is the last barrier preventing the radioactive substances from being released into the environment. The PCCS is used to maintain the integrity of the containment under the design basis accidents, such as loss of coolant (LOCA) or main steam line break (MSLB). After the accident occurs, large volumes of high-temperature gases and steam are released to the containment system. The PCCS is activated and utilizes a separate heat pipe to transmit heat into the water tank arranged outside of the containment. Therefore, the flow and boiling characteristics of the evaporator of the separate heat pipe are critical and determine whether the system can stably carry a large amount of heat away from the containment.

The separated type heat pipe operates differently from the ordinary heat pipe. The adiabatic riser and the downcomer connect the evaporator and the condenser to each other. Therefore, the separated type heat pipe forms a closed natural circulation loop and two-phase vapor-liquid flow in the same direction, eliminating the entrainment limit of the conventional gravity heat pipe and the capillary limit of the capillary heat pipe. The suitable liquid absorbs heat and changes phase in the evaporator, and then fluid reaches the condenser through the riser. In the condenser, the gas phase releases the latent heat and condenses into liquid phase. In response to gravity, the liquid phase returns to the evaporator section again through the downcomer. The difference

* Corresponding author.
E-mail address: wnh@sdu.edu.cn (N. Wang).

https://doi.org/10.1016/j.applthermaleng.2019.03.067
Received 21 October 2018; Received in revised form 21 February 2019; Accepted 11 March 2019
Available online 13 March 2019
1359-4311/

Nomenclature

c_p	specific heat (kJ kg^{-1} K^{-1})
D	diameter of tube (mm)
E	energy (J kg^{-1})
F_V	interface-induced volume force (N)
g	gravity acceleration (m s^{-2})
h	heat transfer coefficient (W m^{-2} K^{-1})
h_{fg}	latent heat (J kg^{-1})
M	molecular weight of vapor
m	mass transfer (kg m^{-3} s^{-1})
P	pressure (Pa)
R	universal gas constant (8.314 J mol^{-1} K^{-1})
L	length (mm)
S	volumetric mass source term
S_h	heat source term
T	temperature (K)
t	time (s)
v	velocity (m s^{-1})

Greek symbols

α	volume fraction
ρ	density (kg m^{-3})
κ	interface curvature
σ	surface tension coefficient
λ	effective thermal conductivity (W m^{-1} K^{-1})
μ	dynamic viscosity (kg m^{-1} s^{-1})
ν	kinematic viscosity (m^2 s^{-1})
η	thermal expansion coefficient
φ	correction factor
γ	accommodation coefficient

Subscripts

l	liquid phase
v	vapor phase
δ	molecular
sat	saturated temperature

density of the fluid between the evaporator and the condenser is the driving force of the heat pipe. The heat transfer of the pipe mainly depends on the latent heat absorbed or released through the fluid phase change [6].

Many researchers have investigated flow boiling in a tube. According to the experimental data, different researchers have proposed formulas for calculating the heat transfer coefficient of a saturated nucleate boiling in a vertical tube. Because the vertical tube saturated nucleate boiling process is similar to the pool boiling process, previous researchers directly fitted the relationship according to the experimental data and variables [7], and other calculation formulas [8,9] were composed of the pool boiling heat transfer and the flow boiling heat transfer calculation formulas after the corrections were added separately. However, boiling heat transfer involves many parameters. The proposed model and empirical correlation have their own limitations and differ widely. Especially in the case of low heat flux, boiling in the tube is similar to the pool boiling process. Chen [10] proposed a mechanism of micro and macro-convective heat transfer to represent boiling heat transfer with net vapor generation to saturated, nonmetallic fluids in convective flow. Gungor et al. [11] reported that even for quite modest vapor qualities, the void fraction was high and the boundary layer next to the wall was thin. An enhancement factor was added to the nucleate boiling term. Chen et al. [12] studied flow boiling instability in a single macro-channel under low pressure natural circulation. They found that the dynamic interactions between the heated channel and upstream compressible volume lead to a long period and large amplitude flow instabilities. Jo et al. [13] used potential gradient and kinetics of superheated liquid to investigate bubble nucleation on smooth surfaces with different wettabilities, and verified this theory through experimental. The results provided fundamental understanding of the incipient boiling.

For the heat transfer in the tube, the bubble shape and heat exchange are interrelated [14]. Kaichiro et al. [15] developed new flow-regime criteria for upward gas-liquid flow in vertical tubes considering the mechanisms of flow-regime transitions. The criteria agree with the existing data for atmospheric air-water flows. Kataoka et al. [16] reported that Taylor bubbles do not exist in large diameters due to their instability. Sateesh et al. [17] argued that sliding bubbles appear at lower heat flux and disappear at a higher heat flux. Okawa et al. [18] studied the bubble rising path in the vertical upward flow boiling process. They found that the bubble rising velocity was comparable to the local velocity and the bubble size was almost constant. The distance between the center of the bubble and the vertical wall rapidly increased due to the variations of the size and shape of a bubble after the nucleation.

Although the empirical correlations can be applied to check the engineering system design scheme, they are valid only within the range obtained from experimental data. Normally, because of the high cost of performing an industrial-scale experiment, it is difficult to properly analyze the boiling state before industrial applications. However, the computational fluid dynamics (CFD) [19,20] can easily be implemented at low cost. Furthermore, numerical simulation has become a feasible and effective method to analyze the local heat transfer characteristics and mechanism.

Juric and Tryggvason [21] simulated liquid-vapor phase change and proposed a numerical method. The method applied to film boiling was found to achieve excellent agreement with experimental results. Kuang et al. [22] simulated the boiling flow behavior in the evaporator of a separated type heat pipe consisting of a bundle of tubes of inner diameter of 65 mm. Pouryoussefi et al. [23] presented an automatic and intelligent system to recognize the two-phase water–air flow regime in a vertical tube based on fuzzy logic and a genetic algorithm. Sato et al. [24] presented a new phase-change model developed from a mass-conservative interface tracking method. The mass transfer rate is directly calculated from the heat flux at the liquid–vapor interface, and the phase change occurs only in the cells that include this interface.

The empirical correlations have been valuable in the design of engineered systems, however, such correlations correspond to the average values of the parameters, not the specific details of the flow. Therefore, the purposes of the present study are the following: (1) to simulate the bubble flow at low flux and study the bubble dynamics of boiling; (2) to simulate local heat transfer characteristics understand the mechanism of flow boiling because the local heat transfer on the tube wall is not distributed uniformly; (3) unlike most simulations, which use small diameter tubes and non-water fluids as the operating conditions, the present study focuses on an intermediate-scale tube and water under a wall superheating condition from 3 to 6 degrees.

2. Mathematical model

The volume of fluid (VOF) model [25] with a user-defined function (UDF) is used for the numerical simulation of boiling flow. The VOF model is applicable for analyzing two or more immiscible fluids flow systems and tracking the volume fraction of each of the fluids. In the present study, the water-vapor phase change will be considered a single event in the tube, and liquid water and vapor are treated as the primary phase and the secondary phase, respectively, for the VOF model.

2.1. Governing equations

To identify the interface location, the tracking of the interface between the phases was accomplished using a continuity equation for the volume fraction of the liquid and vapor phases. For these two phases, the equation has the following form:

$$\frac{1}{\rho_l}\left[\frac{\partial}{\partial t}(\alpha_l\rho_l) + \nabla\cdot(\alpha_l\rho_l\vec{v}) = S_l + \dot{m}\right] \tag{1}$$

$$\frac{1}{\rho_v}\left[\frac{\partial}{\partial t}(\alpha_v\rho_v) + \nabla\cdot(\alpha_v\rho_v\vec{v}) = S_v + \dot{m}\right] \tag{2}$$

where $\dot{m}$ is the mass transfer between the liquid phase and the vapor phase. α_l, α_v represent the liquid volume and the vapor volume fraction, respectively. Only the primary phase volume fraction (the liquid phase) is solved, as the secondary volume fraction field (the vapor phase) is obtained. The volume fractions of the two phases sum to unity:

$$\alpha_l + \alpha_v = 1 \tag{3}$$

The momentum equation and energy equation of the VOF model are shared among the phases. The momentum equation is given below:

$$\frac{\partial}{\partial t}(\rho\vec{v}) + \nabla\cdot(\rho\vec{v}\vec{v}) = -\nabla p + \nabla\cdot[\mu(\nabla\vec{v} + \nabla\vec{v}^{T})] + \rho\vec{g} + F_V \tag{4}$$

where F_V represents interface-induced volume force. The interface-induced volume force in the VOF model is described by the continuum surface force (CSF) model proposed by Brackbill et al. [26] According to the CSF model, the force at the surface can be expressed as a volume force using the divergence theorem. F_V can be written as follows:

$$F_V = \sigma\frac{\alpha_l\rho_l\kappa_v\nabla\alpha_v + \alpha_v\rho_v\kappa_l\nabla\alpha_l}{0.5(\rho_l + \rho_v)} \tag{5}$$

where the surface curvature κ is defined as below:

$$\kappa_l = -\kappa_v = \nabla\cdot\frac{\nabla\alpha_l}{|\nabla\alpha_l|} \tag{6}$$

The energy equation is given below:

$$\frac{\partial}{\partial t}(\rho E) + \nabla\cdot(\vec{v}(\rho E + p)) = \nabla\cdot(\lambda\nabla T) + S_h \tag{7}$$

where the VOF model treats energy, E, in terms of mass-averaged variables:

$$E = \frac{\alpha_l\rho_l E_l + \alpha_v\rho_v E_v}{\alpha_l\rho_l + \alpha_v\rho_v} \tag{8}$$

In addition, the properties ρ, μ and λ are dependent on the volume fractions of two phases:

$$\rho = \rho_l\alpha_l + \rho_v\alpha_v \tag{9}$$

$$\mu = \mu_l\alpha_l + \mu_v\alpha_v \tag{10}$$

$$\lambda = \lambda_l\alpha_l + \lambda_v\alpha_v \tag{11}$$

In the present study, the fluid flow velocity near the inlet is not high. Although heat transfer problems can be successfully solved using the default solution defined by the Reynolds numbers, natural convection with flow boiling using the Reynolds number to determine flow state is not accurate, especially with gravity acting on the density variations. To improve accuracy near the wall region, the Grashof (Gr) number is applied.

$$Gr = \frac{g\eta\Delta TD^3}{\upsilon^2} \tag{12}$$

Furthermore, the realizable k − ε model [27,28] is adopted because its performance is more stable and accurate than that of standard k − ε model.

2.2. Phase-change model

The objective of the phase-change model is to provide the mass source terms S_l and S_v and the energy source term S_h in the local interphase due to the boiling of the liquid, depending on the local temperature field. Schrage [29] replaced the different directions of molecular motion with the molecular flow generated during the evaporation process and expressed the mass flow crossing the interface due to the phase change based on kinetic theory. The mass flow equation is given below:

$$S_\delta = \sqrt{\frac{M}{2\pi R}}\frac{p}{\sqrt{T}} \tag{13}$$

where M is the molecular weight and R is the universal gas constant.

Introducing the correction factor φ to modify Eq. (13) according to the differences between the experimental and theoretical evaporation rates. Therefore, the net mass flux across the interface S is given by the following expression:

$$S = \varphi\sqrt{\frac{M}{2\pi R}}\left[\frac{p_v}{\sqrt{T_v}} - \frac{p_{sat}(T_l)}{\sqrt{T_l}}\right] \tag{14}$$

where the correction factor φ is expressed as Eq. (15):

$$\varphi = \frac{2\gamma}{2-\gamma} \tag{15}$$

The accommodation coefficient γ is defined as the molecules from the bulk phase strike and cross the interface. The accommodation coefficients γ_e and γ_c are the evaporation and condensation coefficients, respectively. If the accommodation coefficient is equal to one, then the condensation or evaporation process is completely condensed or evaporating, otherwise, the vapor or liquid reaching the gas-liquid interface is not all condensed into liquid or evaporated into vapor [30]. When the liquid-vapor interface is in equilibrium, the accommodation coefficients γ_e and γ_c are treated as one parameter [31]. In the present numerical calculation, the accommodation coefficient γ is assumed to be one because the complete phase change has occurred.

The pressure and temperature of the fluid are close to the saturated state at the phase interface, namely, $T_v \approx T_{sat}$ under fluid saturation pressure. The Clausius-Clapeyron equation can be written as follows:

$$p - p_{sat} = \frac{h_{fg}}{T(1/\rho_v - 1/\rho_l)}(T - T_{sat}) \tag{16}$$

Accordingly, Eq. (14) is written as follows:

$$S = \varphi\sqrt{\frac{M}{2\pi RT_{sat}}}\frac{h_{fg}}{(1/\rho_v - 1/\rho_l)}\frac{T - T_{sat}}{T_{sat}} \tag{17}$$

To match the mass source terms S_l and S_v of Eq. (17), Eq. (17) can be simplified by a time relaxation factor parameter β:

$$S_l = \beta_l\alpha_l\rho_l(T - T_{sat})/T_{sat},\ T \leqslant T_{sat} \tag{18}$$

$$S_v = \beta_v\alpha_v\rho_v(T - T_{sat})/T_{sat},\ T > T_{sat} \tag{19}$$

where the time relaxation factors β_l and β_v are set as 0.1 according to the literature [32].

Thus, the energy source term can be realized by the following equation:

$$S_h = h_{fg}S \tag{20}$$

3. Simulation domains and numerical setup

The structures of separate types of heat tube, except the evaporation sections, are not considered in the numerical simulation. Thus the system entry is the evaporator inlet, the outlet is the evaporator outlet, and the system boundary is the outer wall of the evaporator. The

evaporation section is a 5-m-long stainless-steel tube. Because the cross-section of the tube is circular, the entire geometry structure is a strict axisymmetric model. The cross-section of the tube has been able to present the majority of the flow and heat transfer characteristics. Thus the model can be simplified to a two-dimensional model to reduce the amount of calculation. To ensure the accuracy of the flow in the phase change region, the inlet and outlet of the evaporation section are increased to $5D_i$ length extension, as shown in Fig. 1. The tube is filled with saturated water before the start of the calculation. The filling ratio (FR) is defined as the percentage of the volume of the liquid in the capacity of the tube before the evaporator operating. Table 1 shows the specific structural parameters of the model. The boundary conditions are shown in Table 2.The inlet is set as the velocity inlet. No liquid flow into the tube at the beginning of the calculation. And only when the tube is filled with fluid, the inlet liquid flow equal to the flow of the outlet fluid via complete condensation of the separating type heat tube condenser. The outlet is set as the pressure outlet which pressure value equal to the saturation pressure of the vapor. The tube wall is set as the third type of boundary condition, the ambient temperature is 121.82 °C, and the heat transfer coefficient is 998.4 $W m^{-2} K^{-1}$.

To improve the accuracy of the simulation, the wall region mesh is refined due to the high gradients of variables. To investigate grid independency, four different grids were considered as shown in Table 3. The grid with 442,065 meshes was shown to be suitable for further investigation.

The numerical solution is obtained by using the pressure-based finite volume scheme. Pressure-velocity coupling is accomplished through the pressure-implicit with splitting of operators (PISO) method. The least squares cell based method is employed for accurately calculating scalar gradients. The PRESTO method is adopted to discretize the pressure. To ensure keep the interface accuracy, the Geo-Reconstruct method for volume-fraction discretization is adopted in the VOF model with an explicit scheme. The second-order upwind scheme is employed for discretization of both momentum and energy terms. Because of global Courant number restriction, a variable time step (0.00001–0.000075 s) is set to maintain the global Courant number at less than 0.5 in the simulation.

4. Results and discussion

The physical process of flow boiling with low heat flux includes complex interactions of heat and mass transfer. The thermophysical properties and flow characteristics, such as bubble formation, motion, coalescence and breaking along the tube, are revealed in this numerical simulation.

4.1. Validation of the code

The fluid saturation temperature of this simulation is 110 °C, and the result of the average heat transfer coefficient is 3729.39 $W m^{-2} K^{-1}$. The simulation result is compared with the saturated nucleate flow boiling relationship of Forster and Zuber [33] (Eq. (21)) and Chen [10] (Eq. (22)). The results are shown in Table 4. The heat transfer coefficient is greater than the empirical formula, and the errors are 21.3% and 25% compared to the relationships described by Chen and Forster and Zuber, respectively.

$$h = 0.00122\left(\frac{\rho_l^{0.49}\lambda_l^{0.79}c_{pl}^{0.45}}{\sigma^{0.5}\rho_v^{0.24}h_{fg}^{0.24}\mu_l^{0.29}}\right)(\Delta T_o)^{0.24}(\Delta P_o)^{0.75} \tag{21}$$

$$h = 0.00122S\left(\frac{\rho_l^{0.49}\lambda_l^{0.79}c_{pl}^{0.45}}{\sigma^{0.5}\rho_v^{0.24}h_{fg}^{0.24}\mu_l^{0.29}}\right)(\Delta T_{sat})^{0.24}(\Delta P_{sat})^{0.75} + 0.023F\left[\frac{G(1-x)D}{\mu_l}\right]^{0.8}\left(\frac{\mu_l c_{pl}}{\lambda_l}\right)^{0.4}\left(\frac{\lambda_l}{D}\right) \tag{22}$$

where S and F are given below:

$$S = \left(\frac{\Delta T_o}{\Delta T_{sat}}\right)^{0.24}\left(\frac{\Delta p_o}{\Delta p_{sat}}\right)^{0.75} \tag{23}$$

$$F = \left(\frac{Re}{Re_l}\right)^{0.8} \tag{24}$$

The main reason for the difference is that the flow boiling under different conditions (tube diameter, heat flux, tube length, inlet velocity, etc.) is not exactly the same. The boiling mode mainly includes saturated nucleate boiling and forced convective heat transfer under the condition of parameters of intermediate diameter and low heat flow. The Forster and Zuber empirical formula mainly considered the nucleate boiling in the pool boiling condition without considering the influence of the flow heat transfer coefficient. Chen revised Eq. (21) by modifying the mean superheat to wall superheat and adding a forced convection term. His correlation covers both the saturated nucleate boiling region and the two-phase forced-convection region. Chen assumed that both the saturated nucleate boiling and force convection occur to cover the entire range of the correlation. Therefore, he did not distinguish the regimes of heat transfer state along the length of the tube, and the added liquid heat transfer coefficient is not accurate under the low flow rate condition.

In general, the empirical formula can provide a simple calculation method, however, there is no specific analysis of the flow process. The simulation results highlight the detailed features of boiling heat transfer and the flow regime including the local heat transfer coefficient, temperature, phase distribution, and bubble shape.

4.2. Physical field analysis

With the increase of the tube height, the flow pattern and heat

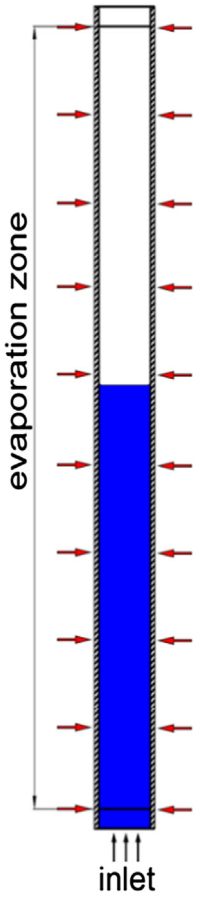

Fig. 1. Physical model.

Table 1
Structural parameters.

Parameter		Numerical value
Inner diameter	D_i(mm)	50
Outer diameter	D_o(mm)	57
Tube length	L(mm)	5000
Filling ratio	FR	53.6%

Table 2
Boundary conditions.

No.	Location	Boundary type
1	Tube inlet	Velocity-inlet
2	Tube outlet	Pressure-outlet
3	Tube outwall	Third type of boundary condition
4	Tube inwall	Coupled

Table 3
Mesh independent validation.

No.	Number of meshes	Heat flux (W m^{-2})
1	251,547	14,518
2	333,751	10,245
3	442,065	11,689
4	536,495	11,546

Table 4
Comparison of the results from other authors and the numerical simulation.

Author	Numerical value	Deviation
Chen [10]	3072.37	21.3%
Forster and Zuber [33]	2983.64	25.0%

transfer characteristics are different at different heights, thus, a change in one leads to a corresponding change in the other. Figs. 2–4 show the distribution of temperature field, phase and velocity fields at different heights inside the tube. From the bottom to the top of the tube, the temperature, velocity, and vapor fraction increase gradually.

At the bottom of the tube, the heat transfer is dominated by subcooled boiling and nuclear boiling after the liquid flows in and small bubbles are formed. Because of the effect of buoyancy-driven motion induced by the temperature gradient, the velocity of the small bubbles flowing upward along the tube wall is higher than the main stream velocity and the small bubbles merge with other small bubbles to grow into larger bubbles. As a bubble grows, it will gradually break away from the tube wall. It is not possible to produce large disturbances due to the low bubble velocity, as a result, the temperature near the wall surface is higher than the temperature of the center fluid.

In the middle region, the effect of buoyancy-driven motion on the flow weakens. The bubbles formed at the tube wall will quickly escape from the wall instead of flowing upward along the wall. Long overheated areas are not formed on the wall surface, and the temperature field inside the tube tends to be even. The cap flow and slug flow are formed with the agglomeration and coalescence of bubbles. However, the cap flow and the slug flow cannot be stabilized as a result of the low heat exchange capacity and the intermediate tube diameter.

As the height increases further, the vapor phase velocity is much higher than that of the liquid phase, and the churn flow is formed in the upper region. The turbulence of the vapor phase makes it easy for the bubbles to cover the wall of the tube and form the overheated area during the flow.

Figs. 5–7 shows the radial distribution of the time-averaged void fraction, the time-averaged gas velocity and the time-averaged liquid velocity at different heights of the tube. The void fraction and velocity magnitude in general are increasing with the increase of height and the radial distributions from a wall-peak shape to a core-peak shape. At the height of 0.25 m, the peak of void fraction and velocity magnitude appear near the wall surface. This situation is caused by the low velocity of the fluid entering the tube and the weak intensity of the nucleate boiling at the wall, causing the thermal buoyancy-driven process to dominate the bottom flow. Near the height of 0.75 m, the radial distribution of void fraction tends to be average, however, the void fraction is slightly lower near the wall because the large bubbles agglomerated at the wall gradually move away from the wall and enter the main stream and the small bubbles in the main stream are also growing and gathering. As the height increases to approximately 2 m, the bubble flow begins to develop into the cap flow and slug flow gradually. The void fraction and velocity magnitude showed the highest value at the location at approximately r/R = 0.7 because the flow pattern around this height does not entirely correspond to cap bubble flow but, rather, to developing cap bubble flow affected by the tube diameter. At the heights of 3.5 m and 4.5 m, the core-peak shapes of the radial distribution of the void fraction and the velocity magnitude become steeper as the flow pattern changes from slug flow to churn flow.

Fig. 8(a)–(e) show the velocity vectors and flow diagrams at different heights of the tube. Figs. 8(a) and 9(a) shows the bottom of the tube, where the flow regime is dominated by bubbly flow. Influenced by the buoyancy-driven motion, the velocity of the bubble near the wall is faster than the velocity of the bubble away from the wall as shown in Fig. 6. The bubbles are elongated under the effects of the tension, buoyancy force and tangential force of main stream field. A small dispersed bubble moves upward along the tube without significant local chaotic bubble motion. The bubbles moving along the wall are gradually separated from the wall as shown in Fig. 8(b). As small bubbles agglomerate and coalesce, cap bubbles will gradually form. Once the cap bubbles are formed, each cap bubble randomly collides with other bubbles, and each cap bubble is constantly expanding. As shown in Figs. 8(c) and 9(b), the cap bubbly region exhibits local chaotic motion,

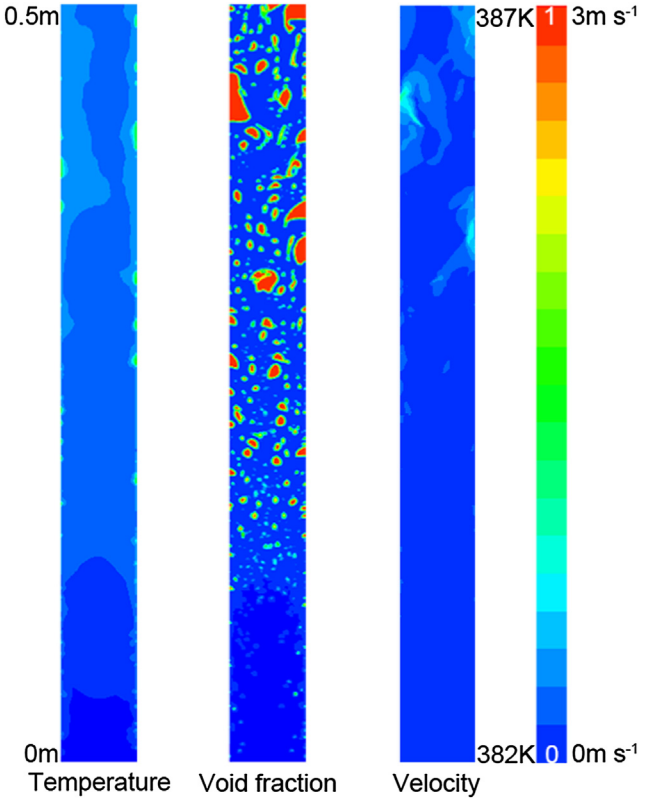

Fig. 2. The physical field in the lower part.

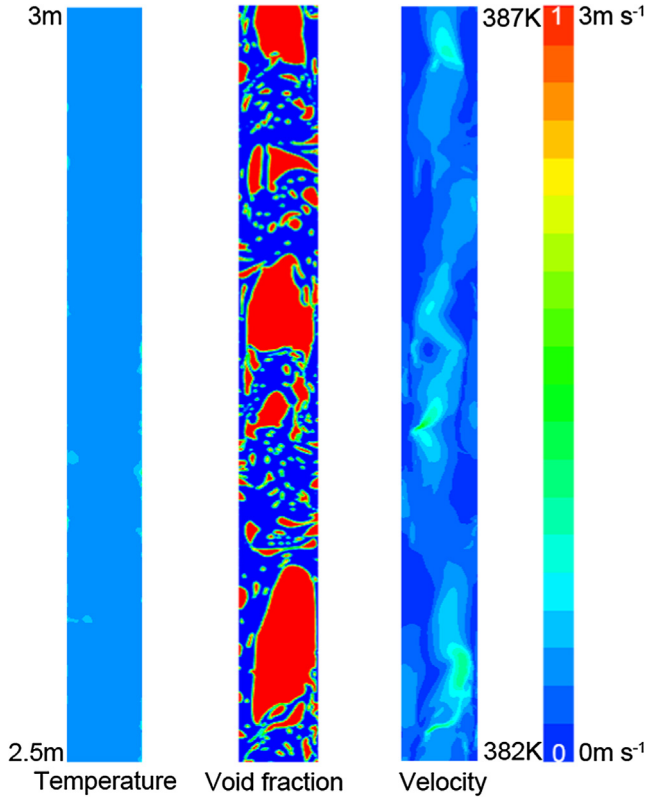

Fig. 3. The physical field in the middle part.

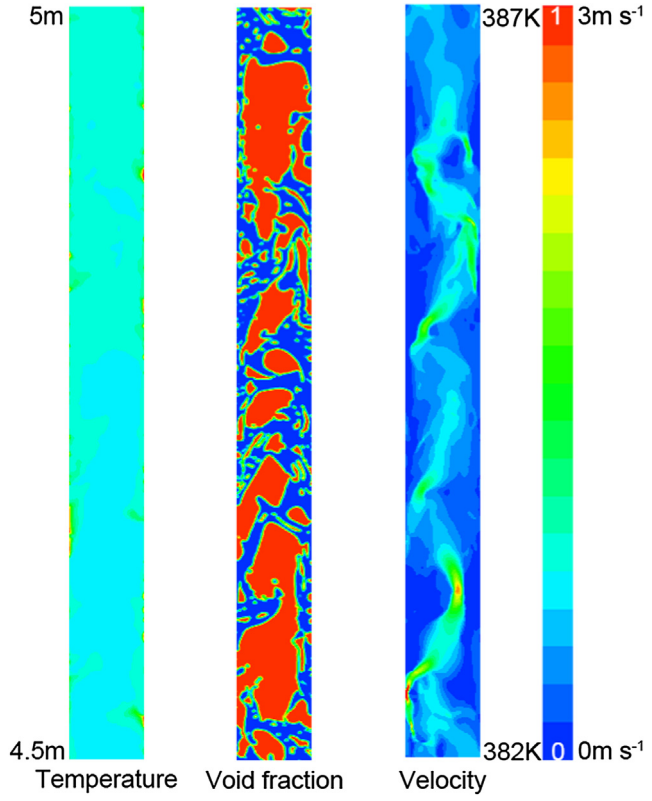

Fig. 4. The physical field in the upper part.

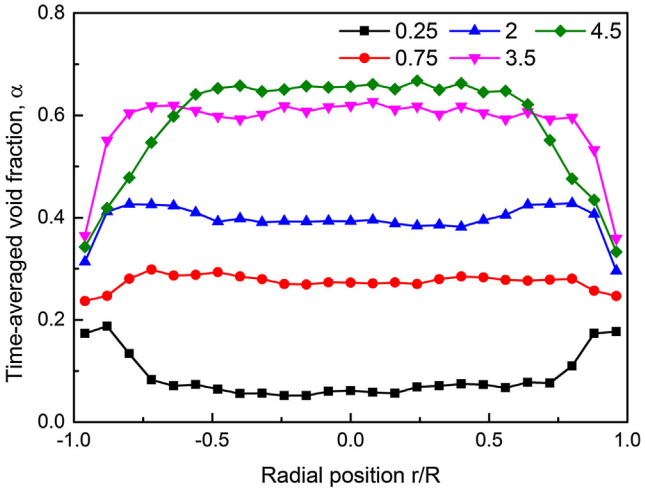

Fig. 5. Radial distribution of time-averaged void fraction.

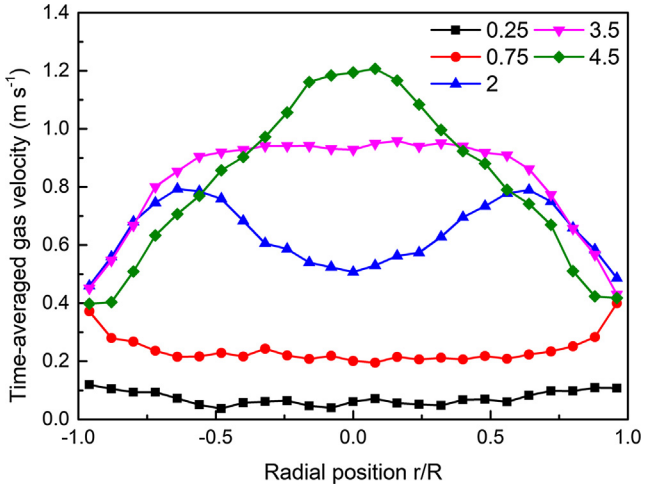

Fig. 6. Radial distribution of time-averaged gas velocity.

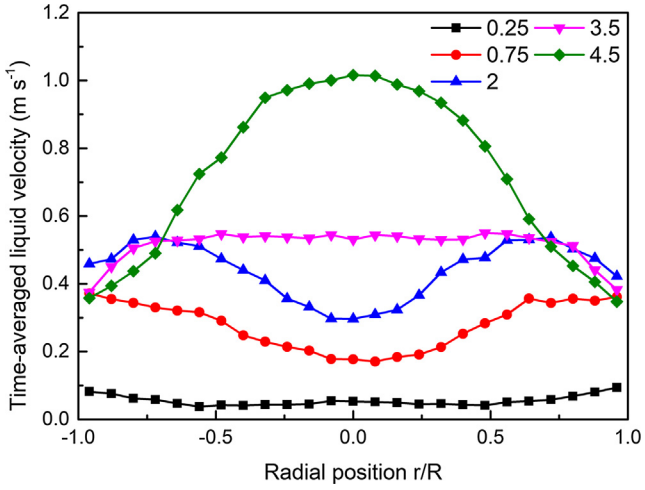

Fig. 7. Radial distribution of the time-averaged liquid velocity.

namely, co-existence of upward and downward flows of bubbles and liquid. Moreover, the cap bubbles always maintain irregularly deformed shapes and cannot maintain a size close to the tube cross-section because shear force and interfacial instability increase probability of the breakup of the large cap bubbles. The slug flow regime appeared at high superficial gas velocity conditions, as shown in Fig. 8(d), and developed from the large coalescent cap bubbles. Many small bubbles follow the tail of the slug bubble. As the void fraction of the tube rises,

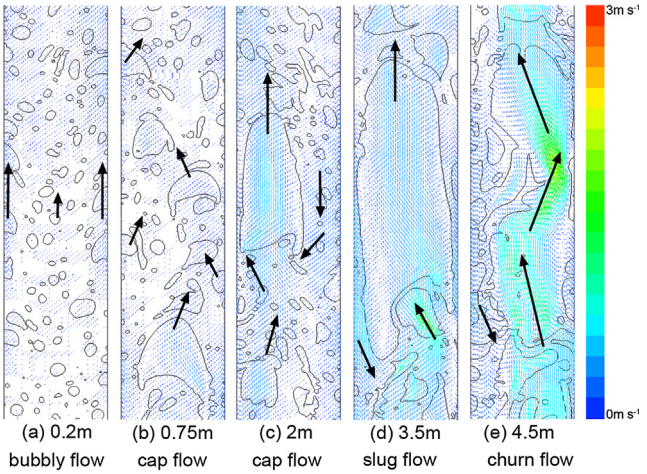

Fig. 8. The local velocity vector and flow regime.

the slug flow cannot be stabilized and the flow rapidly converts to churn flow. The churn flow shown in the flow regimes of Figs. 8(e) and 9(c) is composed of relatively large deformed bubbles, with the bubble structure distorting when moving upward. The liquid phase flows downward and close to the bubbly path, whereas the vapor phase pushes upward and connects rapidly. The churn bubbles agitate the flow, producing strong local turbulence and secondary flow.

4.3. Characteristics of the heat transfer

The boiling heat transfer coefficient is not invariable as time increases, however, it is closely related to the flow state and vapor phase distribution of the tube. Therefore, it is necessary to discuss the time-averaged characteristics of the boiling heat transfer. Fig. 10 shows the average heat transfer coefficient of the left and right wall surfaces at different times. The heat transfer coefficient fluctuates with time, and the change value is inconsistent at the same time on both sides of the tube. The vapor phase distribution is not uniform under an intermediate-scale tube, continuous and stable cap flow and slug flow cannot be formed, as shown in Fig. 8. Especially at the upper part of the tube, the flow regime gradually enters the churn flow, whether the bubble covers the wall will directly affect the heat transfer coefficient. Therefore, the heat transfer coefficients of the left wall and right wall show different degrees of fluctuation. If the time coordinate of Fig. 10 is adjusted, there will also be a moment when the right wall fluctuates greatly.

During the time period selected in Fig. 10, the fluctuation range of the left wall heat transfer coefficient is greater than the right wall. It shows that at the peak and valley value on the left side, the flow pattern and vapor phase distribution in the tube are more intense for heat transfer. To further obtain the relation between the fluctuation of the heat transfer coefficient and the surface coverage fraction of the vapor, the times t1 and t2 at the peak and valley values of the adjacent heat transfer coefficient of the left wall of the tube are analyzed. The length of the tube is divided into 10 sections, with each part of the length of 0.5 m, to analyze heat transfer performance. As shown in Figs. 11 and 12, the value of the vapor surface coverage fraction affects the heat transfer coefficient of the wall. As the height increases, the coverage fraction also increase due to the transition of the flow state in the tube from the bottom bubble flow to the upper churn flow. In the 0–0.5, 0.5–1, and 1–1.5 intervals, the coverage fraction and heat transfer coefficient at time t_1 are very similar to those at time t_2. The flow regime in these three sections is mainly dominated by bubble flow and cap flow, and the bubble disturbance is weak. In the sections of 2–2.5, 2.5–3, 3–3.5, there is a difference in the coverage fraction between times t_1 and t_2, and the change trend of heat transfer coefficient is also

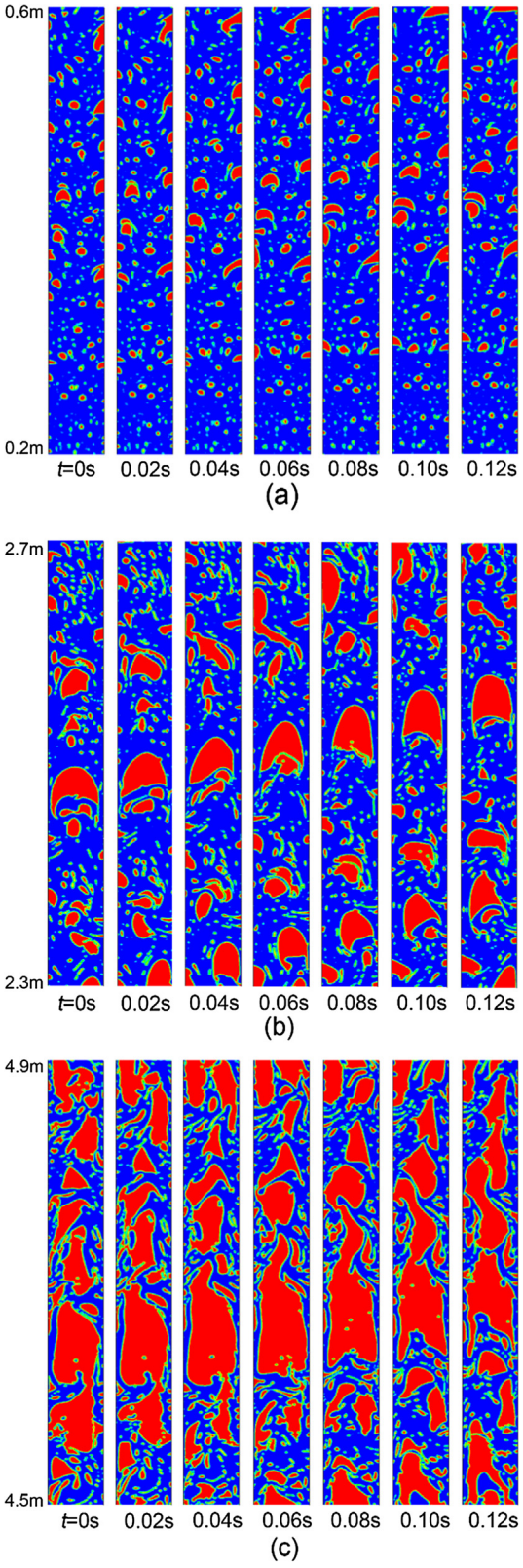

Fig. 9. The images of the flow pattern development over time.

different. In these three sections, the slug flow and large cap flow alternately appear, and the flow field inside the tube is significantly disturbed by the influence of bubble agglomeration and fragmentation. Starting from the height of 3.5 m, the flow regime gradually enters the churn flow, and the wall surface of the tube is covered with bubbles,

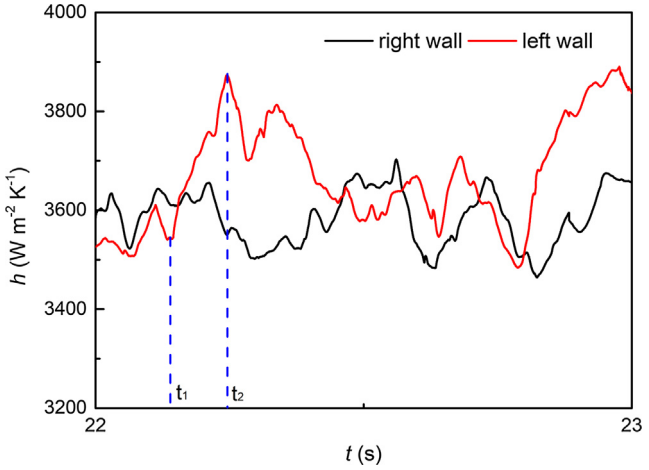

Fig. 10. Transient and time-average heat transfer coefficients on the tube wall.

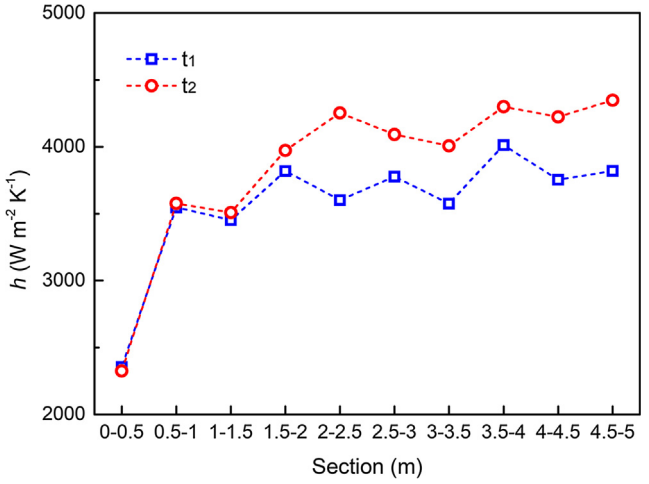

Fig. 11. The heat transfer coefficient on the wall of tube sections.

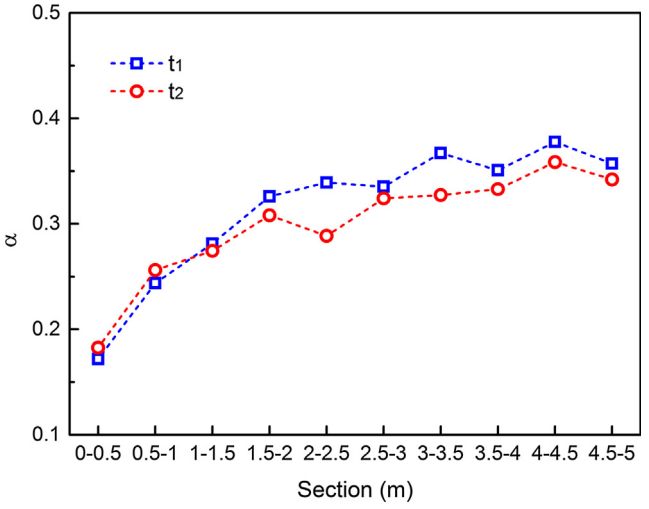

Fig. 12. The coverage void fraction on the tube wall.

this situation easily forms a superheated area to reduce heat exchange. The flow pattern is not similar to the forced convection forming the liquid film under high heat flow conditions, the vapor cannot push the liquid to the wall to form an annular flow, only forming the discontinuous liquid film. But overall, the heat transfer coefficient increases with the growth of the tube length.

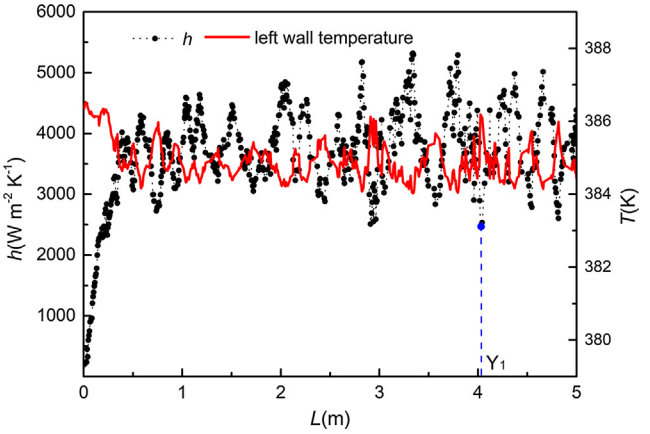

Fig. 13. The instantaneous distribution of the heat transfer coefficient and the wall temperature.

Fig. 13 shows the instantaneous distribution of the heat transfer coefficient and the wall temperature along the length of the left wall at time t1. As the length of the tube increases, the flow pattern undergoes bubble flow, cap flow, slug flow and churn flow. In the inlet section of the tube, the boiling intensity is weaker and the tube wall temperature is higher, the heat transfer type is dominated by subcooled boiling. As the heat flux is increased, the wall temperature decreases, more nucleation sites are activated and the number of boiling surfaces increases until nucleate boiling is fully developed. The heat transfer coefficient fluctuates less in the lower half of the tube (L < 2 m), and the fluctuation becomes greater as the agitation increases via the increase of bubble sizes. In the upper part of the tube, the slug flow and churn flow cause the discontinuous liquid film at the wall surface, and convection boiling of the liquid film gradually appeared. Moreover, crush and agitation of slug flow and churn flow produce strong local turbulence and secondary flow. These bubble behaviors further improve heat transfer. The valley value of the heat transfer coefficient near Y1 = 4 m is caused by vapor covering the surface, as shown in Fig. 14; when the vapor breaks away from the wall, the heat exchange will be strengthened.

The nucleate boiling and force convective heat transfer occur simultaneously in the tube with low flow flux and heat flux. Fig. 15 shows the heat flux of the different superheating conditions. The entire region can be divided into two areas. In zone I, as the heat flux is increased, more nucleation sites are activated and the number of boiling surfaces increases until fully developed nucleate boiling. The heat flux becomes lower in zone II, the tube wall must reach a higher

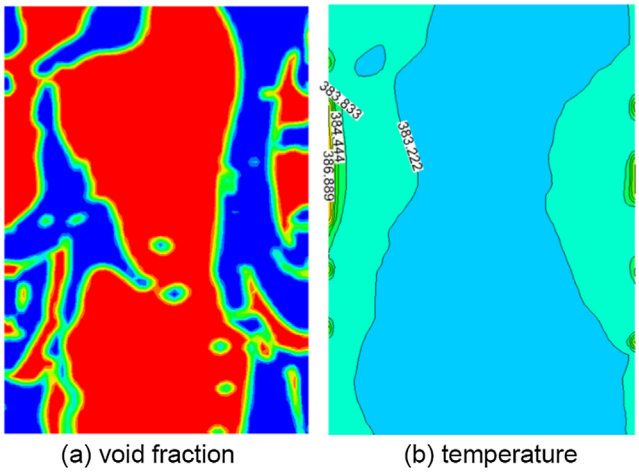

Fig. 14. Phase and temperature distribution at Y_1 = 4 m.

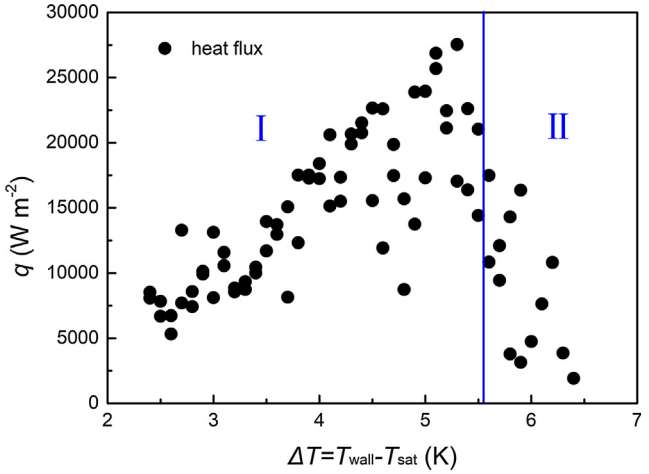

Fig. 15. Heat flux at different superheating conditions on the wall.

superheating condition to maintain nucleate boiling process. The superheating condition basically occurs in the area above 4 m of the tube, in the churn flow regime, and the bubbles easily cover the wall surface to form the wall overheating and boiling pattern that develops the force convective heat transfer gradually. Therefore, the heat transfer is mainly affected by the flow state in zone II.

5. Conclusion

In this paper, the characteristics of boiling heat transfer in a tube under intermediate diameter and low heat flow conditions are studied via numerical simulation. The numerical results confirm the influences of tube diameter and tube length on the saturated nucleate boiling process and show the local characteristics of flow and heat transfer. The important characteristics and parametric trends are as follows.

(1) The temperature field, phase distribution and flow field are obviously different at different heights.
(2) The flow pattern of boiling varies along the tube height. The bubbly flow, cap flow and churn flow patterns appear in the lower part, middle part and upper part of tube, respectively.
(3) The interaction between the flow pattern and the heat transfer regime reflect the characteristics of boiling. The increased superheat improves the nuclear boiling intensity, and the increase in the void fraction causes fluctuations in the heat transfer coefficient.
(4) The heat transfer rate increases at the entrance of the tube, and the heat transfer coefficient increases as the tube length increases. Most of the regions are dominated by saturated nucleate boiling.

Acknowledgements

Funding for this research was provided by the Natural Science Foundation of Shandong Province (Project No.: ZR2016EEM38). The scientific calculations in this paper have been done on the HPC Cloud Platform of Shandong University.

References

[1] H. He, et al., Efficiency enhancement of a loop thermosyphon on a mixed-wettability evaporator surface, Appl. Therm. Eng. 123 (2017) 1245–1254.
[2] C. Yue, Q. Zhang, Z. Zhai, L. Ling, CFD simulation on the heat transfer and flow characteristics of a microchannel separate heat pipe under different filling ratios, Appl. Therm. Eng. 139 (2018) 25–34.
[3] Z. Yang, J. Shan, J. Gou, M. Ishii, SGTR analysis on CPR1000 with a passive safety system, Nucl. Eng. Des. 332 (2018) 319–328.
[4] Y. Li, H. Zhang, J. Xiao, J.R. Travis, T. Jordan, Numerical investigation of natural convection inside the containment with recovering passive containment cooling system using GASFLOW-MPI, Ann. Nucl. Energy 114 (2018) 1–10.
[5] M.H. Kusuma, et al., Passive cooling system in a nuclear spent fuel pool using a vertical straight wickless-heat pipe, Int. J. Therm. Sci. 126 (2018) 162–171.
[6] A.J.P. Zimmermann, C. Melo, Two-phase loop thermosyphon using carbon dioxide applied to the cold end of a Stirling cooler, Appl. Therm. Eng. 73 (2014) 547–556.
[7] R.W. Bjorg, G.R. Hall, W.M. Rohsenow, Correlation of forced convection boiling heat transfer data, Int. J. Heat Mass Transf. 25 (1982) 753–757.
[8] S.G. Kandlikar, A general correlation for saturated two-phase flow boiling heat transfer inside horizontal and vertical tubes, J. Heat Transf. 112 (1990) 219.
[9] Z. Liu, R.H.S. Winterton, A general correlation for saturated and subcooled flow boiling in tubes and annuli, based on a nucleate pool boiling equation, Int. J. Heat Mass Transf. 34 (1991) 2759–2766.
[10] J.C. Chen, Correlation for boiling heat transfer to saturated fluids in convective flow, Ind. Eng. Chem. Process Des. Dev. 5 (1966) 322–329.
[11] K.E. Gungor, R.H.S. Winterton, A general correlation for flow boiling in tubes and annuli, Int. J. Heat Mass Transf. 29 (1986) 351–358.
[12] X. Chen, P. Gao, S. Tan, Z. Yu, C. Chen, An experimental investigation of flow boiling instability in a natural circulation loop, Int. J. Heat Mass Transf. 117 (2018) 1125–1134.
[13] H.J. Jo, M. Kaviany, S.H. Kim, M.H. Kim, Heterogeneous bubble nucleation on ideally-smooth horizontal heated surface, Int. J. Heat Mass Transf. 71 (2014) 149–157.
[14] Y. Tian, Z. Chen, N. Wang, D. Zhou, L. Cheng, Numerical and experimental investigation of pool boiling on a vertical tube in a confined space, Int. J. Heat Mass Transf. 122 (2018) 1239–1254.
[15] M. Kaichiro, M. Ishii, Flow regime transition criteria for upward two-phase flow in vertical tubes, Int. J. Heat Mass Transf. 27 (1984) 723–737.
[16] I. Kataoka, M. Ishii, Drift flux model for large diameter pipe and new correlation for pool void fraction, Int. J. Heat Mass Transf. 30 (1987) 1927–1939.
[17] G. Sateesh, S.K. Das, A.R. Balakrishnan, Analysis of pool boiling heat transfer: effect of bubbles sliding on the heating surface, Int. J. Heat Mass Transf. 48 (2005) 1543–1553.
[18] T. Okawa, An experimental study on bubble rise path after the departure from a nucleation site in vertical upflow boiling, Exp. Therm. Fluid Sci. 29 (2005) 287–294.
[19] C.R. Kharangate, I. Mudawar, Review of computational studies on boiling and condensation, Int. J. Heat Mass Transf. 108 (2017) 1164–1196.
[20] Y. Tian, K. Zhang, N. Wang, Z. Cui, L. Cheng, Numerical study of pool boiling heat transfer in a large-scale confined space, Appl. Therm. Eng. 118 (2017) 188–198.
[21] D. Juric, G. Tryggvason, Computations of boiling flows, Int. J. Multiph. Flow 24 (1998) 387–410.
[22] Y.W. Kuang, W. Wang, R. Zhuan, C.C. Yi, Simulation of boiling flow in evaporator of separate type heat pipe with low heat flux, Ann. Nucl. Energy 75 (2015) 158–167.
[23] S.M. Pouryoussefi, Y. Zhang, Identification of two-phase water-air flow patterns in a vertical pipe using fuzzy logic and genetic algorithm, Appl. Therm. Eng. 85 (2015) 195–206.
[24] Y. Sato, B. Ničeno, A sharp-interface phase change model for a mass-conservative interface tracking method, J. Comput. Phys. 249 (2013) 127–161.
[25] C.W. Hirt, B.D. Nichols, Volume of fluid (VOF) method for the dynamics of free boundaries, J. Comput. Phys. 39 (1981) 201–225.
[26] J.U. Brackbill, D.B. Kothe, C. Zemach, A continuum method for modeling surface tension, J. Comput. Phys. 100 (1992) 335–354.
[27] T.-H. Shih, W.W. Liou, A. Shabbir, Z. Yang, J. Zhu, A new k-epsilon eddy viscosity for high Reynolds number turbulent flows, Comput. Fluids 24 (1995) 227–238.
[28] S.E. Kim, D. Choudhury, B. Patel, Computations of complex turbulent flows using the commercial code FLUENT, Model. Complex Turbul. Flows 7 (1999) 259–276.
[29] R.W. Schrage, A Thermal Study of Interface Mass Transfer, Columbia University Press, New York, 1953, pp. 160–256.
[30] R. Marek, J. Straub, Analysis of the evaporation coefficient and the condensation coefficient of water, Int. J. Heat Mass Transf. 44 (2001) 39–53.
[31] A. Faghri, Y. Zhang, Front Matter-Transport Phenomena in Multiphase System, Academic Press, San Diego, 2006, pp. 450–501.
[32] M. Magnini, B. Pulvirenti, J.R. Thome, Numerical investigation of hydrodynamics and heat transfer of elongated bubbles during flow boiling in a microchannel, Int. J. Heat Mass Transf. 59 (2013) 451–471.
[33] H.K. Forster, N. Zuber, Dynamics of vapor bubbles and boiling heat transfer, AIChE J. 1 (1955) 531–535.